Absolute Frequency Measurement of Thallium $6P_{1/2} \rightarrow 7S_{1/2}$ Transitions Using Optical Femtosecond Comb

Wei-Ling Cheng
National Tsing Hua University

July 12, 2005

Abstract

Absolute frequency measurement of thallium $6P_{1/2} \rightarrow 7S_{1/2}$ transitions using optical femtosecond comb

Wei-Ling Cheng

National Tsing Hua University, Taiwan 2005

The Doppler-free spectroscopy of atomic thallium $6P_{1/2} \rightarrow 7S_{1/2}$ transitions have been observed by centering the Lamb dip using two counter-propagating laser beams perpendicular to the atomic beam, and the absolute frequencies of these transitions have been measured to an accuracy of 0.4 MHz (1 ppb) using the optical femtosecond comb. The hyperfine splittings and isotope shifts are derived from our results, which are in agree with the previous experimental results, and improved by a factor of 2–3.

Contents

List of Figures

List of Tables

Chapter 1

Introduction

1.1 Motivation

Now atomic parity nonconservation (PNC) has been measured using various atomic species, such as: bismuth [1], lead [2, 3], thallium [4, 5], and cesium [6]. Analysis of the data provides an important test of the standard electroweak model in low-energy regime and imposes constraints on new physics beyond the standard model. So far, experiments are in excellent agreement with atomic structure calculations of the current theory. The accuracy of both experiments and the theory is best for cesium [6, 7, 8]. In thallium, a new round of atomic structure calculations has been completed [9], and this calculation must be check with the energy level experiment. Thallium also plays an important part in measurement of electron's electrical dipole moment (EDM) [10]. Measurements of violations of fundamental symmetries in atoms, such as PNC and EDM, are very effective means of testing of the standard model of elementary particles and searching new physics beyond it [11].

Parity nonconservation (PNC) in atoms arises largely due to the interaction (exchange $Z^0 - boson$) between atomic electrons and the nucleus. The weak electron-nucleus interaction violates parity, but conserves time-reversal. The nuclear weak charge, Qw, give the largest contribution to parity violation in heavy atoms compared to other mechanisms. However, the interpretation of the measurements in heavy atoms is strongly impeded by the poor knowledge of the atomic wave func-

tions. These atomic structure calculations requires a variety of independent atomic structure measurements— such as hyperfine structure, energies and electric dipole transition amplitudes —of high precision to provide cross-checks on accuracy and guide the development of the theory. A comparison of the calculated and experimental values gives an indication of the quality of the many-body wave functions.

Thallium is the heaviest stable element with a single p-electron outside closed shells. The electron configuration for the ground state of thallium is $6s^2 6p_{1/2}$. It can be treated as one-electron or three-electron system above close shell. However, its $6p$ electron is close to the $6s$ electrons, and correlations between those two states are significant. This means that the calculation for thallium will be more complicated then for cesium, which is with a single s-electron outside closed shells.

The level energy of thallium is a important bench mark for its atomic structure calculation. For example, the isotope shift is caused by the mass and field shift, which is related to the value of the electronic wave function at nuclei, $\delta\langle r^2\rangle$, the change in the mean-square charge radius between the nuclei. An accurate estimate of the charge radius can be deduced, with atomic structure calculations of high precision [12].

Atomic PNC effects depend intimately on the behavior of the electron wave function near the nucleus. Also, hyperfine structure is sensitive to the wave functions at small distance from the nucleus. Hyperfine splitting (HFS) and isotope shift (IS) measurements can provide important information concerning the nuclei. These level energy measurements, contain HFS and IS measurements, can serve as very useful tests of the theory and those are developing.

Finally, hyperfine anomaly and isotope shift measurements can serve as tests of nuclear structure calculations. The distribution of charge and of nuclear magnetic moment both affect the hyperfine structures. As pointed out in [13], models of nuclear magnetic moment distributions can be tested via measured hyperfine anomalies. Such a comparison may have implications for so-called "Schiff moments" used in interpretation of experiments searching $P-$ and $T-$violating effects [14].

1.2 Energy Level of Thallium and Laser Induced Fluorescence

The atomic number of thallium is 81. Natural thallium consists two isotopes of masses 203 and 205, both with nuclear spin $I = 1/2$. The natural abundance of ^{203}Tl and ^{205}Tl is 30% and 70%, respectively. Fig. 1.1 shows partial energy level diagram and Grotrian diagram for thallium. The ground state involves a single electron in a p-shell ($6^2P_{1/2}$ state). The $6P_{3/2}$ state is metastable state with a long lifetime (0.23 sec [15]), since the transition $6P_{3/2} \rightarrow 6P_{1/2}$ is $E1$ forbidden. The ground state hyperfine splitting is 21 GHz, so that in thermal equilibrium the relative populations are almost equal at room temperature. The transition probability, $A_{ki}[10^8 s^{-1}]$, of the $7S_{1/2} \rightarrow 6P_{1/2}$ (377-nm) and $7S_{1/2} \rightarrow 6P_{3/2}$ (535-nm) is 0.625 and 0.705, respectively. The Λ-type level structure in atomic thallium results in several interesting phenomena. In a 377-nm optical pumping experiment, the population will eventually be trapped in the metastable state.

In the visible and ultraviolet regions a very high sensitivity spectroscopy can be achieved, if the absorption of laser photon is monitored through laser-induced fluorescence (LIF). When the laser is tuned to an absorbing transition, the number of photons absorbed per second is proportional to the number of fluorescence photons emitted per second from the excited state. LIF serves as a sensitive monitor for the absorption of laser photons in fluorescence excitation spectroscopy [16]. Fig. 1.2 shows the hyperfine structure and $6P_{1/2,3/2} - 7S_{1/2}$ transitions of thallium. When the laser frequency is tuned to the absorbing transitions $6P_{1/2} \rightarrow 7S_{1/2}$, detection of fluorescence from the excited level $7S_{1/2}$ to metastable state $6P_{3/2}$ achieves fluorescence excitation spectroscopy of thallium.

1.3 Optical Femtosecond Comb System

An optical femtosecond comb was used for absolute frequency measurement of transitions in fluorescence excitation spectroscopy of thallium. Optical femtosecond comb

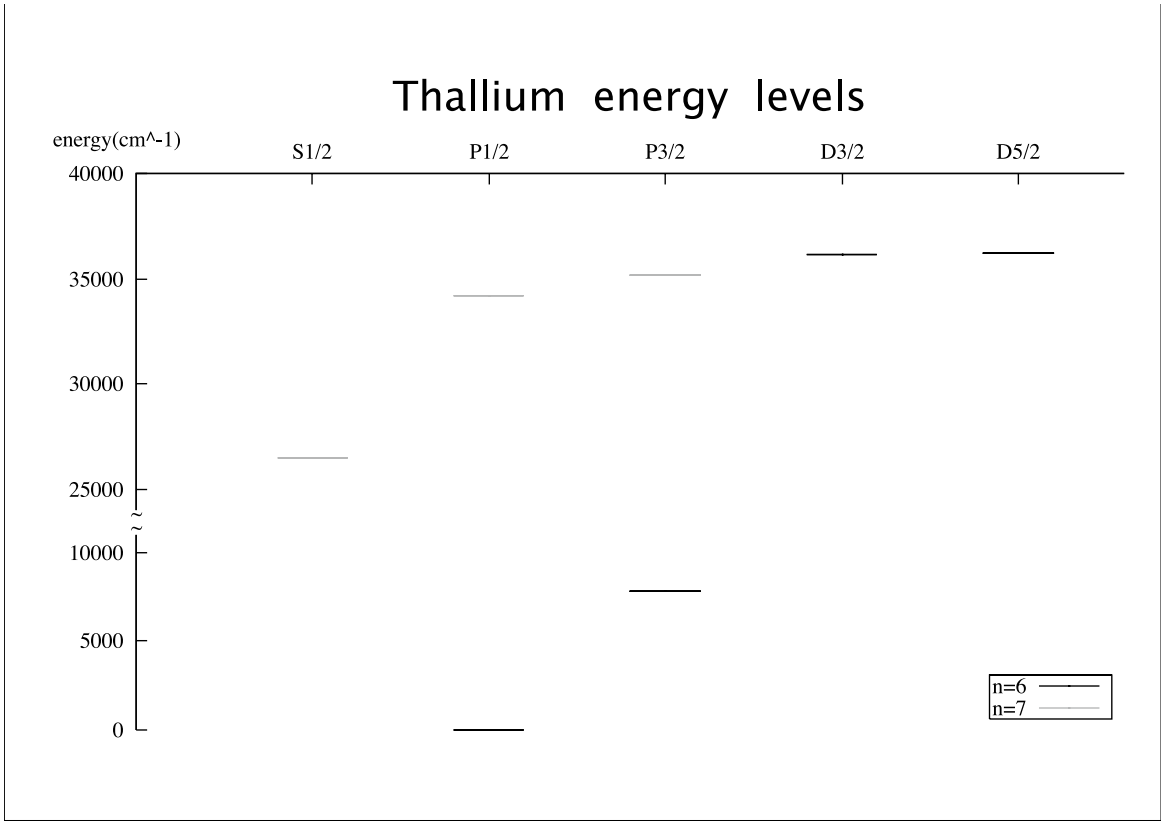

Figure 1.1: Diagram of atomic energy levels and Grotrian diagram for thallium.

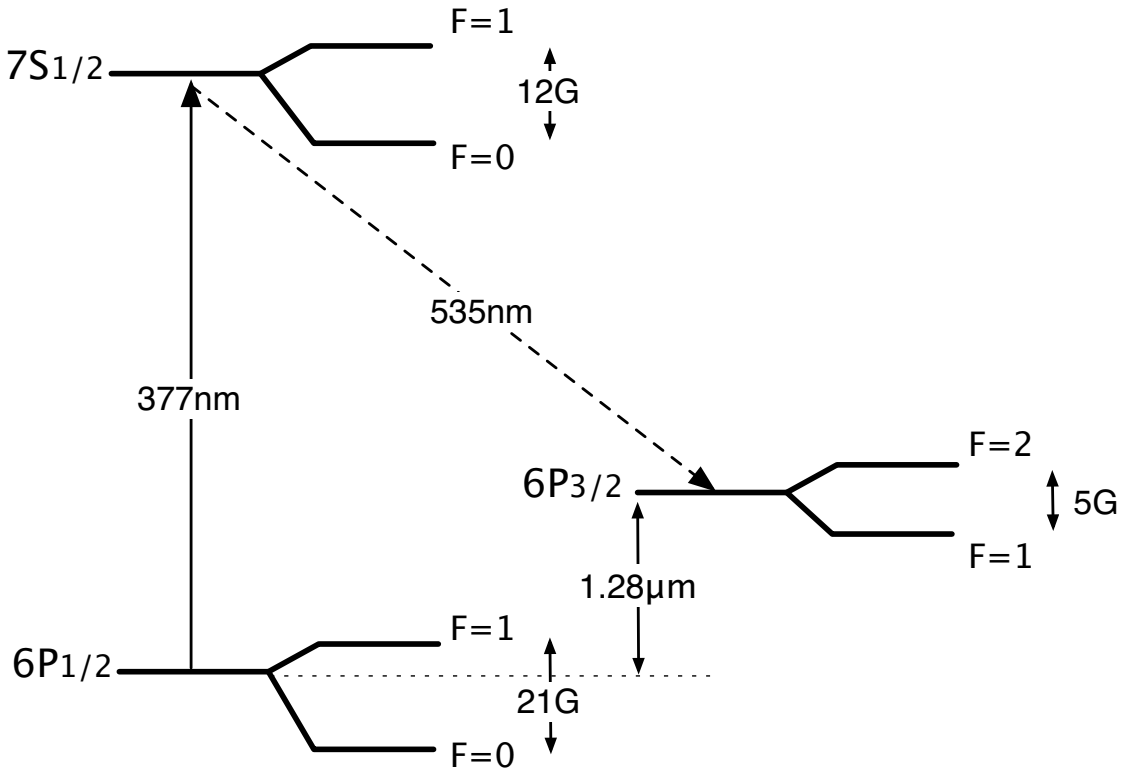

Figure 1.2: Partial energy level diagram of thallium. (not scaled)

is a revolutionary technique in determining the optical absolute frequency. It is like a frequency "ruler" to measure any unknown frequency within the optical region. It bases on the technique of optical frequency synthesizer with femtosecond laser frequency comb [17], which a phase-controlled femtosecond mode-locked Ti-Sapphire laser is used. The absolute frequency can be measured by beating the femtosecond comb lines with unknown laser source. The laser frequency can be calculated with a simple equation $f = N \times f_{rep} \pm f_o \pm f_{beat}$. The f_{rep} is the pulse repetition frequency of a mode-locked laser which is locked on an atomic frequency standard. f_o is another important parameter of comb, offset frequency. The N value is determined by the wavemeter with the accuracy of GHz. The absolute frequency can be measured by the beatnote, f_{beat}, with the femtosecond comb lines.

Chapter 2

Experiment

2.1 Experiment Setup

The experimental setup is shown in Fig. 2.1. A collimated atomic beam is irradiated perpendicularly by the frequency-doubled 755-nm Ti-sapphire. The atomic beam source is an effusion oven containing thallium. The transition is detected using the 535-nm fluorescence with a photo-multiplier (PMT). A small portion of 755-nm laser beam is picked up using a blank glass plate, and sent to optical femtosecond comb through a single mode optical fiber. A reference cavity with a FSR=300 MHz is used to monitor when laser is scanning. The absolute frequency of laser is also measured using a home-made wavemeter with GHz accuracy.

2.1.1 Laser Source

The UV light source schema is shown in Fig. 2.2. The fundamental laser light at 755-nm is provided by a Coherent MBR-110 Ti-sapphire, pumped by a 10W Verdi solid-state laser at 532-nm. The 755-nm laser is frequency-doubled in a LBO crystal with a enhance ring cavity. A Brewster cut LBO crystal [18], $3 \times 3 \times 10$ mm^3, is placed midway between the two curved mirrors, where the primary wist is located. The LBO crystal is mounted on a three-axis rotational stage to optimize the phase matching condition. Coupling lenses are in front of the SHG cavity and achieve phase-matching.

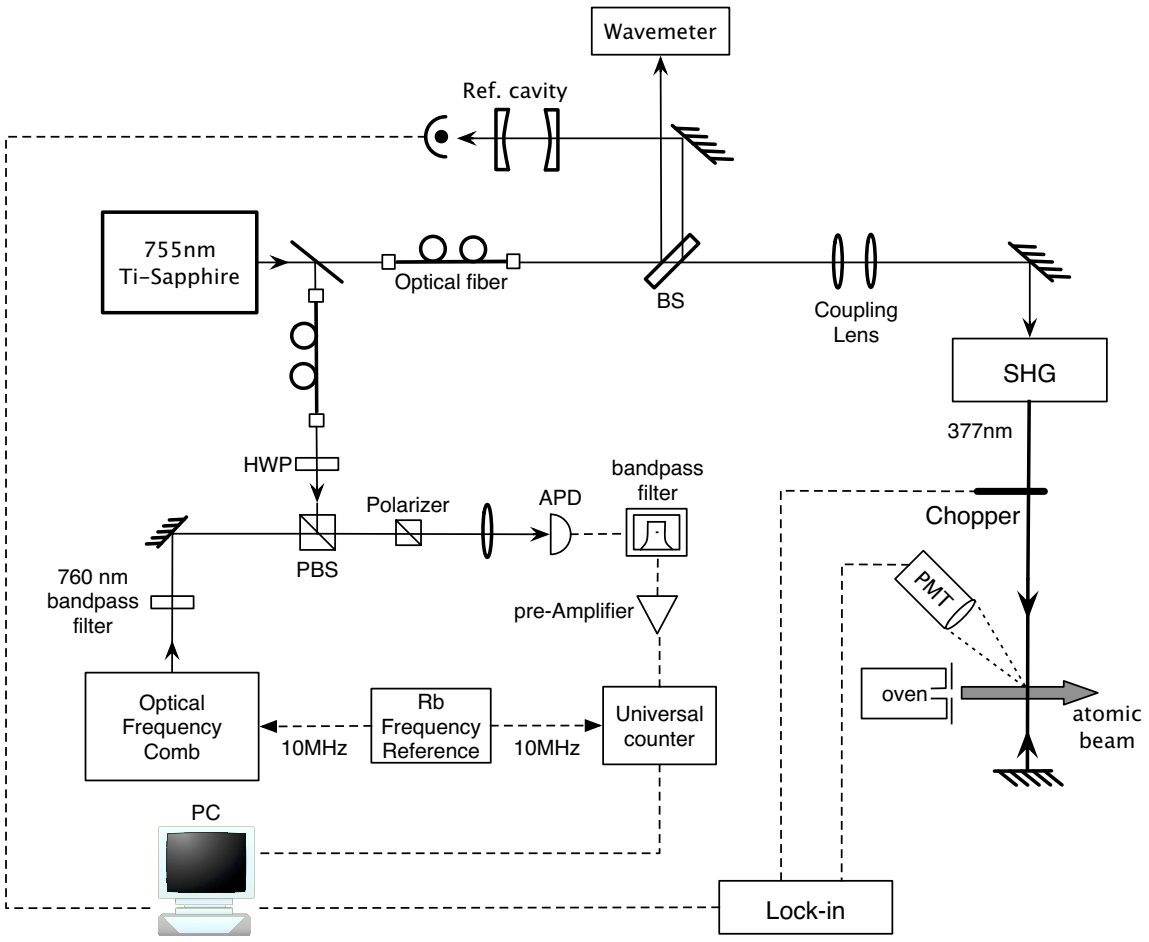

Figure 2.1: The experimental setup of absolute frequency measurement of thallium $6P_{1/2} \rightarrow 7S_{1/2}$ transition

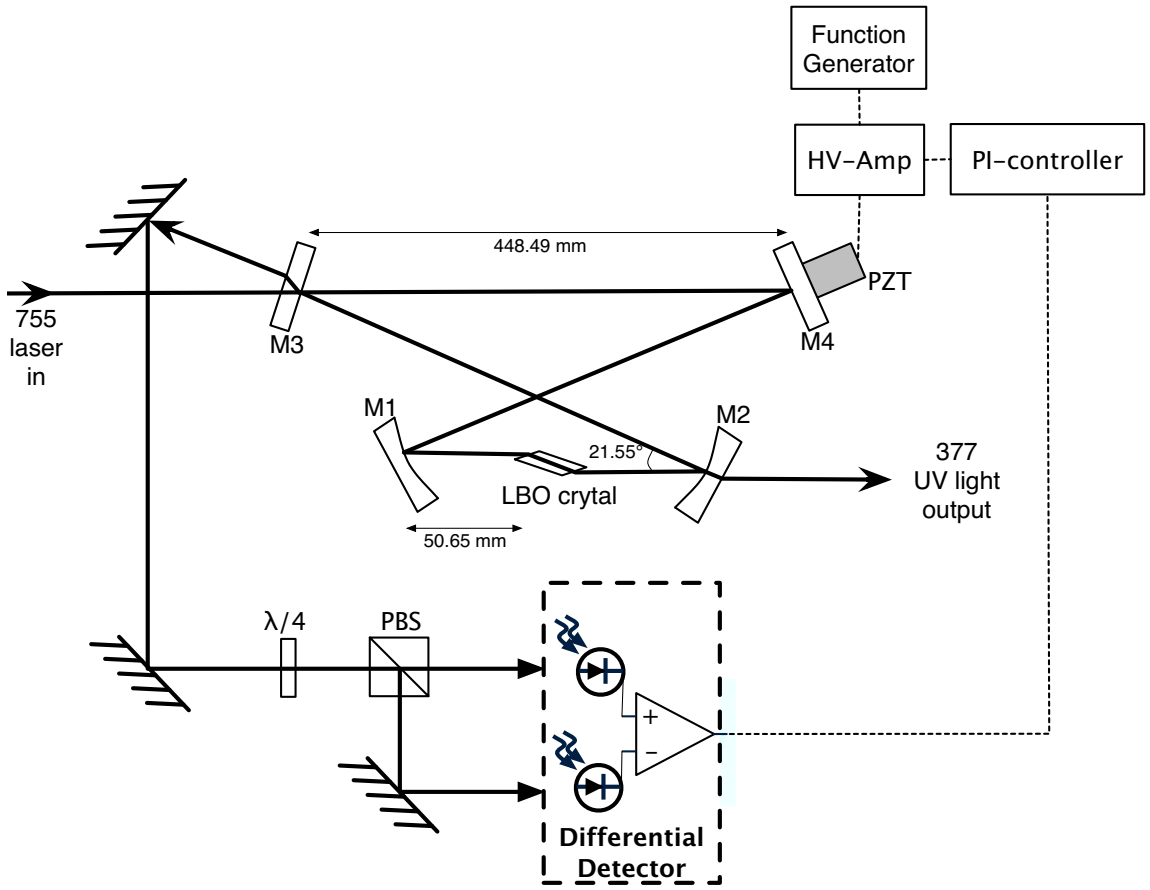

Figure 2.2: Experimental setup of the doubling cavity. The cavity is locked to the fundamental laser light using a Hänsch-Couillaud locking technique which employs a quarter-wave plate ($\lambda/4$), a polarizing beamsplitter (PB) and two photodiodes (PD). Specification of optical components of enhance cavity is listed in Table. 2.1.

Our servo-locking system bases on the technique of polarization rotation [19]. The power output of optical fiber is about 200 mW. The frequency-doubled light is less than 1 mW, but is enough to probe the atomic beam. The output laser beam size is collimated to 2 mm $\times$ 10 mm.

2.1.2 Oven and Atomic Beam

Atomic beam technique increases the spectral resolution and reduces the Doppler broadening effect by using a collimated beam with reduced transverse velocity component, and provides a collision-free environment. The disadvantage of the technique is the low number density and low signal strength [20]. The thermal atomic beam is

Table 2.1: Specification of optical components of enhance cavity

component	Description
M1	BK7 curved mirror, Dia 12.7 × 6 mm, ROC 100 mm, HR@740-770 nm, R> 99.5%.
M2	FS curved mirror, Dia 12.7 × 6 mm, ROC 100 mm, HR@740-770 nm, R> 99.5%, HT/AR@370-385 nm, T> 80%.
M3	BK7 flat coupler, Dia 12.7 × 6 mm, AR/R=97 ± 0.5%@740-770 nm.
M4	BK7 flat thin mirror, Dia 12.7 × 1 mm, HR@740-770 nm, R> 99.5%.
$\lambda/4$	Quartx retardation plate, multi order, AR/AR@755 nm

generated from thallium bulk, which is heated to 450 °C in a vacuum chamber of 10^{-6} torr. The aperture of atomic beam is 2 mm and the velocity of thallium atom is $\sim$ 300 m/s. The residual Doppler boardening, due to the beam divergence, is estimated to 26 MHz in our system [21].

Using two counter-propagating laser beams can eliminate the linear Doppler shift. Two counter-propagating light beams result opposed Doppler shift and the Lamb dip. Absolute transition frequency measurement could be achieved by measuring the center of Lamb dip, without Doppler shift.

2.1.3 Optical Femtosecond Comb System

The optical femtosecond comb system in this experiment is built by the professor Shy's group (NTHU, Taiwan). It bases on the technique of optical frequency synthesizer with femtosecond laser frequency comb. The setup of optical femtosecond comb is shown in Appendix B. The universal counter and the frequency synthesizer are externally referenced to the rubidium frequency standards. A 760 nm bandpass filter is used to filter out the unnecessary femtosecond comb lines and avoid the optical damage of the photodiode as shown in Fig. 2.1. The universal counter counts beatnote of one of femtosecond comb line and 755-nm laser light. The frequency fluctuation of the stabilized repetition frequency is 4 mHz. The stabilized offset frequency fluctuation

is 11 mHz when it is locked. The total frequency fluctuation is kHz when $N = 10^5$. The accuracy of this femtosecond comb system is 10^{-11} [22, 23].

2.2 Data Acquisition and Histogram

The transition is detected by measuring the 535-nm fluorescence with a photo-multiplier (PMT). A 535-nm filter is placed before PMT. A small portion of 755-nm laser beam is picked up using a blank glass plate, and sent to optical femtosecond comb through an single mode optical fiber. At the same time, the computer records the beat frequency and the fluorescence signal thought lock-in amplifier while laser is scanning. A single scan consists of 500–1200 data points within the frequency range of 50–120 MHz in terms of laser frequency.

The laser frequency can be calculated with a simple equation :

$$f_{unknown} = N \times f_{rep} \pm f_{offset} \pm f_{beat} \ ,$$

where f_{rep} is $\sim$1 GHz. N is a large integer of the order 10^5. f_{offset} and f_{beat} is several hundred MHz. The N value is roughly determined by the home-made wavemeter with the accuracy of GHz. Comparing several different f_{offset} scans in same transmission, the N and the sign of f_{offset} and f_{beat} can be determined. The final histogram of a single transition is a combination of several different scans and data sets. The errorbar of the histogram is given by the standard deviation of the signal of the same laser frequency. Figure 2.3 shows the histogram of all measurements of ^{203}Tl $6P_{1/2} - 7S_{1/2}$ ($F = 0 \rightarrow F = 1$) transition. The errorbar is the standard deviation that averaging the signal of the same laser frequency, and the binning is 1 MHz.

The spectrum is fitted to a combination of two Viogt and a Lorentzian functions:

$$\begin{aligned} S = & A_1 * Voigt(\omega_0 - \omega_{shift}, w_L, w_{G1}) \\ & + A_2 * Voigt(\omega_0 + \omega_{shift}, w_L, w_{G2}) \\ & - A_3 * Lorentzian(\omega_0, w_L) \\ & + C \ . \end{aligned} \tag{2.1}$$

The Voigt function is a convolution of Gaussian

$$Gauss\,(x) = \frac{1}{\sqrt{2\pi}\sigma} \exp\left(-\frac{x^2}{2\sigma^2}\right) \tag{2.2}$$

and Lorentzian functions

$$Lorentz\,(x) = \frac{1}{\pi}\frac{lg/2}{x^2 + lg^2/4} \ , \tag{2.3}$$

lg is the full width of the Lorentz at half its maximum heigh and σ is the half width of the Gauss at half its maximum heigh. A program written in ROOT (from CERN) runs the fitting routine (see Appendix A). Two Viogt functions refer to two fluorescence signals excited from two counter-propagating light. A Lorentzian function with minus sign describes the *Lamb dip*. The center of the Lamb dip is a sensitive marker for the exact center of the atomic transition.

The frequency uncertainty is estimated by:

$$(\Delta f_{unknown})^2 = (N \times \Delta f_{rep})^2 + (\Delta f_{offset})^2 + (\Delta f_{beat})^2 \ . \tag{2.4}$$

The frequency fluctuation of the stabilized repetition frequency is 4 mHz, so the uncertainty of the absolute frequency measurement due to first term $(N \times \Delta f_{rep})$ is on the order of 2 kHz. The stabilized offset frequency fluctuation is 11 mHz. The predominant uncertainty of the absolute frequency measurement in this work is due to the uncertainty of beat frequency, Δf_{beat}. Δf_{beat} is the standard deviation from histogram data. Eventually, we take the fitting error as our absolute frequency

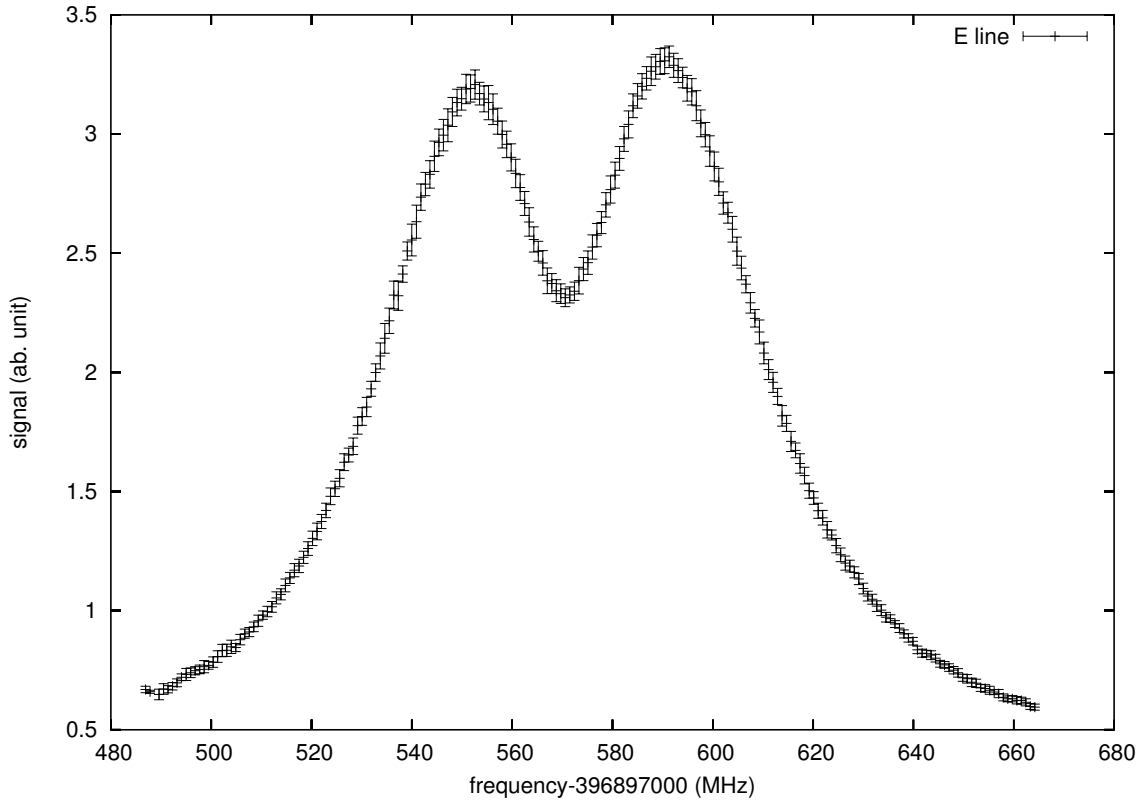

Figure 2.3: The histogram of ^{203}Tl $6P_{1/2} - 7S_{1/2}$ ($F = 0 \rightarrow F = 1$) transition. The frequency axis shown in this figure is the frequency of fundamental laser, not the doubled UV light.

uncertainty.

Chapter 3

Data and Analysis

3.1 Systematic Effect

The Linear Doppler Shift

The linear Doppler shift is given as:

$$\Delta\omega = \vec{k} \cdot \vec{v} \ ,$$

and

$$\Delta\nu = \frac{v}{c}\nu_0 \sin\varphi \ .$$

The experimental results suggest that $\Delta\nu$ is $\sim$15 MHz and the angle between laser and atomic beam, φ, is $\sim$38 mrad. This angle is consistent with our experimental setup. However, this shift has no effect on the absolute frequency measurement, which is determined using the Doppler-free Lamb dip.

The Quadratic Doppler Effect

The counter-propagating laser beams and Lamb dip can eliminated the linear Doppler effect, but not the quadratic one. The quadratic Doppler shift (second-order Doppler effect)

$$\Delta\nu = \frac{v^2}{2c^2}\nu_0$$

is on the order of 200 Hz. Such small frequency shift effect does not need to be taken into account in the accuracy of current experiment.

The Transit-time Broadening

The transit time $T = d/v$ of atoms is the mean thermal velocity v passing through a lsaser beam of diameter d, 2 mm. The transit-time broadening is therefor on the order of v/d, and is $\sim$0.1 MHz with d=2 mm in this work.

Linewidth

The Doppler width of the Voigt profile is on the order of 20 MHz in agreement with the collimation ratio of the atomic beam, which is about 40 mrad. However, the Lorentzian width of the Lamb dip is found to be broadened to 42 MHz (for ^{205}Tl $F = 1 \rightarrow 0$). This is much larger than the transitions natural width of 2.5 MHz. The origin is discussed below.

3.1.1 Saturation and Power Broadening

At sufficiently large laser intensities, the optical pumping rate on an absorbing transition becomes larger than the relaxation rates. This results in a noticeable decrease of the population in the absorbing levels. This saturation of the population densities also causes additional line broadening. The effect of optical pumping on the saturation of population densities is often illustrated by a closed two-level system. And the linewidth of a power-broadened Lorentzian line profile is

$$\gamma_S = \gamma\sqrt{1+S} \ .$$

γ is the natural linewidth. S is the saturation parameter ,

$$S = \frac{2\sigma_{12}I(\omega)}{\hbar\omega A_{12}} \ .$$

The saturation intensity I_s is the intensity at which the saturation parameter S become $S = 1$. The saturation intensity I_s for Tl $6P_{1/2} \rightarrow 7S_{1/2}$ is 9 mW/cm^2 which is much larger than our UV laser source. However, the Lorentzian part of the Voigt profile is found to be broadened to 42 MHz for ^{205}Tl $F = 1 \rightarrow 0$ transition. This is much larger than the transitions natural width of 2.5 MHz. We have found the strong broadening effect is due to the *open two-level system* of the thallium atomic structure.

The population density of atoms in the absorbing level is decreased by optical pumping. This results in a nonlinear dependence of the absorbed radiation power on the incident power. In an open two-level system Fig.3.1, the *saturation parameter*

$$S = \frac{B_{12}\rho_\nu}{R^*} \ , \tag{3.1}$$

with

$$R^* = \frac{R_1 R_2}{R_1 + R_2} \ ,$$

gives the ratio of induced transition probability $B_{12}\rho_\nu$ to the "mean" relaxation probability R^* [16]. It is not proportional to the life time of upper level any longer. *In this Λ-type level structure of atomic thallium optical pumping experiment, the population will eventually be trapped in the metastable state.* That is, the $6P_{1/2} \rightarrow 7S_{1/2}$ can be easily saturated by a very weak laser power.

In a atomic beam, collisions are generally negligible and the excited level decays by spontaneous emission. If the absorbing level is the ground state, the only repopulation mechanisms of absorbing level are the diffusion of atoms into the excitation volume. The "lifetime" is given by by the transit time $T = d/v$ through the excitation region of length d.

Since the fluorescence from $7S_{1/2}$ to $6P_{3/2}$ is the signal detected and the initial population density of $6P_{3/2}$ is considered to be zero, the final population density of $6P_{3/2}$ indicate the total fluorescence photon received. The absorption of the incident wave causes population changes of the levels involved in the laser-atom interaction process. We simulated the population density changes of the levels by solving the rate equations numerically.

The rate equations for $6P_{1/2}$ $(F = 1) \rightarrow 7S_{1/2}$ $(F = 0)$ transition (Fig. 3.2) are:

$$\frac{dN_2}{dt} = -B_{23} \times N_2 \times \rho + B_{32} \times N_3 \times \rho + A_{32} \times N_3 \tag{3.2}$$

$$\frac{dN_3}{dt} = B_{23} \times N_2 \times \rho - B_{32} \times N_3 \times \rho - A_{32} \times N_3 - A_{35} \times N_3 \tag{3.3}$$

$$\frac{dN_5}{dt} = A_{35} \times N_3 \tag{3.4}$$

where N_2, N_3 and N_5 refer to $6P_{1/2}$, $7S_{1/2}$ and $6P_{3/2}$ states respectively, the ρ refers to energy density and the Einstein coefficients (see section 1.2 on page 3) are:

$$\begin{aligned} A_{32} &= 1.56 \times 10^7 \quad \mathrm{s}^{-1} \\ A_{35} &= 1.76 \times 10^7 \quad \mathrm{s}^{-1} \\ B_{32} = B_{23} &= 3.18 \times 10^{13} \quad \mathrm{s}^{-1} \ . \end{aligned}$$

The rate equation is solved numerically by *mathmatica* with the initial conditions:

$$\begin{aligned} N_2 &= 0.75 \\ N_3 &= 0 \\ N_5 &= 0 \ , \end{aligned}$$

and assuming incident laser light power is 0.1 mW, the laser beam size is 2 mm $\times$ 10 mm. The laser beam diameter passing though atomic beam is 2 mm, so the transition time is 6.6 μ second. Fig. 3.3 and Fig. 3.4 show the simulation of populations changes while the laser was tuned to $6P_{1/2}$ $(F = 1) \rightarrow 7S_{1/2}$ $(F = 0)$ optical pumping transition.

In order to simulated the broadening effect, we solved the rate equation numerically, and referred the final population of $6P_{3/2}$ state as the signal strength. Fig. 3.5 shows the signal strength v.s. laser detune. With a laser power of 0.1 mW, the broadening has reached a FWHM of 6 MHz. Fig. 3.6 shows the broadening effect with an incident laser light power of 1 mW, and the broadening has reached a FWHM of 25 MHz. This "*saturation broadening*" is much larger than the absorption transitions natural width, and stronger than conventional "close two-level system".

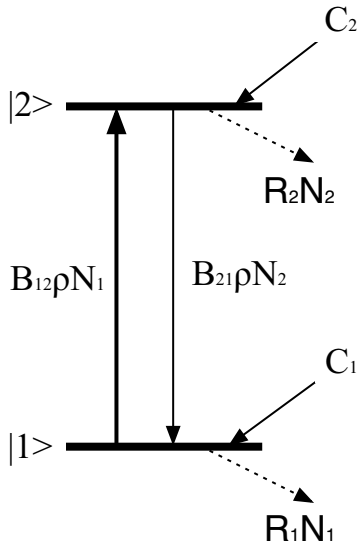

Figure 3.1: Level diagram of an open two-level system with open relaxation channels into other levels and population paths from outside the system.

3.2 Results and Discussion

Fig.3.8–Fig.3.13 show all fitting results, the laser frequency we measured is infrared, not atomic transition frequency—UV light. The accuracy is sub-MHz, and the signal-to-noise ratio (S/N) is ~ 50. The FHWM of Lamb dip is $\sim$30 MHz and the resolution is sub-MHz. The final absolute frequency measurements of thallium $6P_{1/2} - 7S_{1/2}$ transition are listed in Table. 3.1. The six lines are labeled $A - F$ for identification on Table. 3.1 and Fig.3.7. The D-line was measured on a different day from others.

3.2.1 HFS, IS and the Mean Square Isotopic Change $\lambda_{c,m}$

Our hyperfine splitting and isotope shift measurements are in good agreement with the previous experimental results as can be seen in Table. 3.2. From our measured values of the hyperfine constant A_{205} and A_{203}, we can deduce the hyperfine anomaly $\Delta \equiv [(A_{205}/A_{203})(g_{203}/g_{205}) - 1]$, where the g is refer to the nuclear g factor of the relevant isotope. Using the magnetic moments [31] $^{203}\mu = 1.62225787\mu_N$ and $^{205}\mu =$

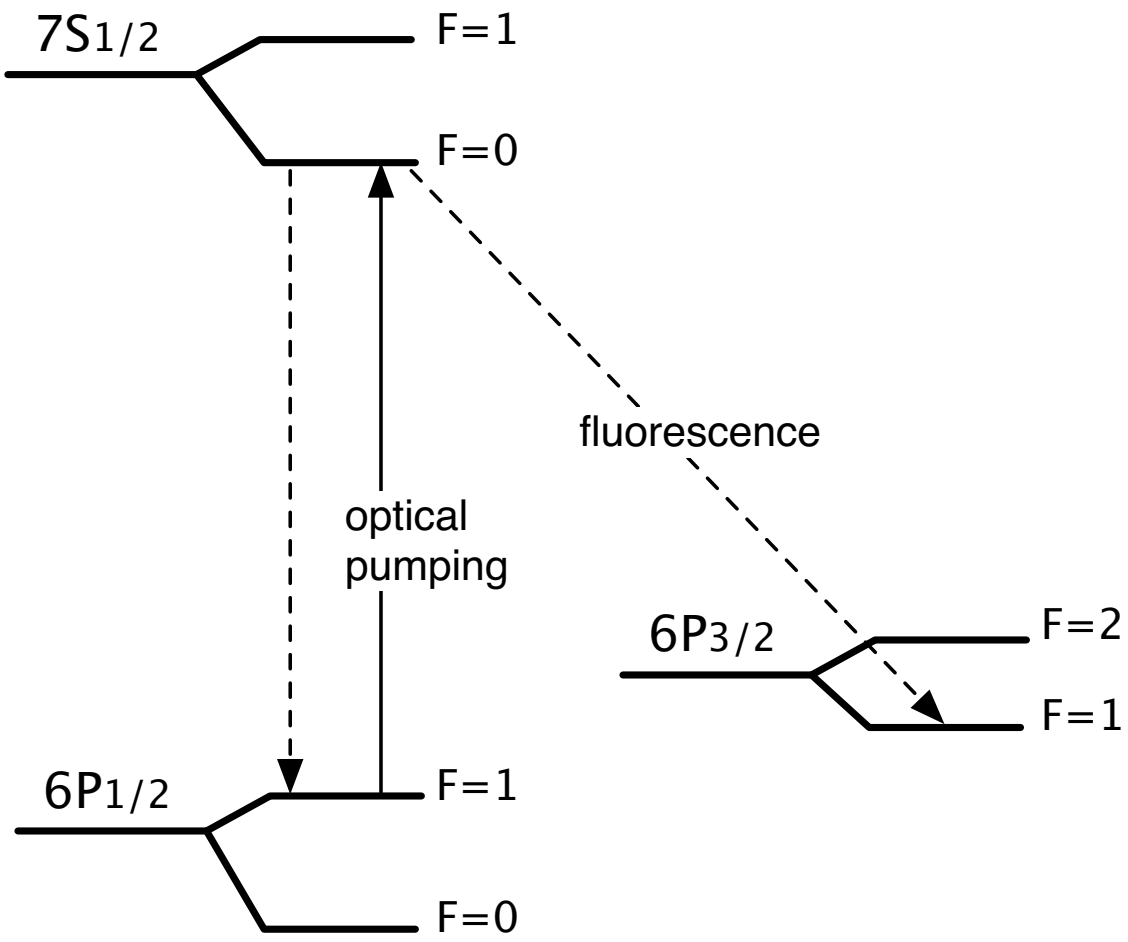

Figure 3.2: The Λ-type level structure of atomic thallium optical pumping

Table 3.1: The transition frequencies of $6P_{1/2} \rightarrow 7S_{1/2}$.

Line	Transition	Laser frequency (MHz)
A	^{203}Tl F=1-0	793 761 854.8 (4)
B	^{205}Tl F=1-0	793 763 375.6 (4)
C	^{203}Tl F=1-1	793 774 035.0 (6)
D	^{205}Tl F=1-1	793 775 671.0 (4)
E	^{203}Tl F=0-1	793 795 140.6 (4)
F	^{205}Tl F=0-1	793 796 982.4 (8)
Pre. expt.[24]	$6P_{1/2} \rightarrow 7S_{1/2}$	793 775.5 (GHz)
Theor.[9]	$6P_{1/2} \rightarrow 7S_{1/2}$	793 100(10) (GHz)

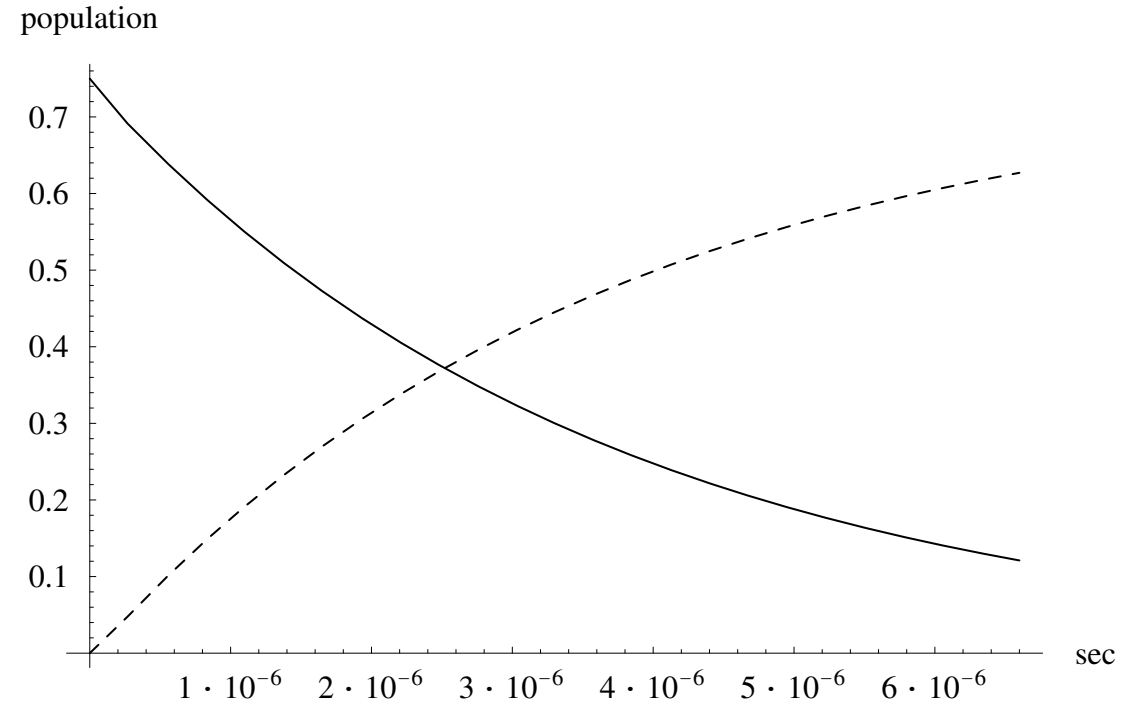

Figure 3.3: The population changes vary with times. The solid line is referred to $6P_{1/2}$ $(F = 1)$. The dashed line is referred to $6P_{3/2}$ $(F = 1)$.

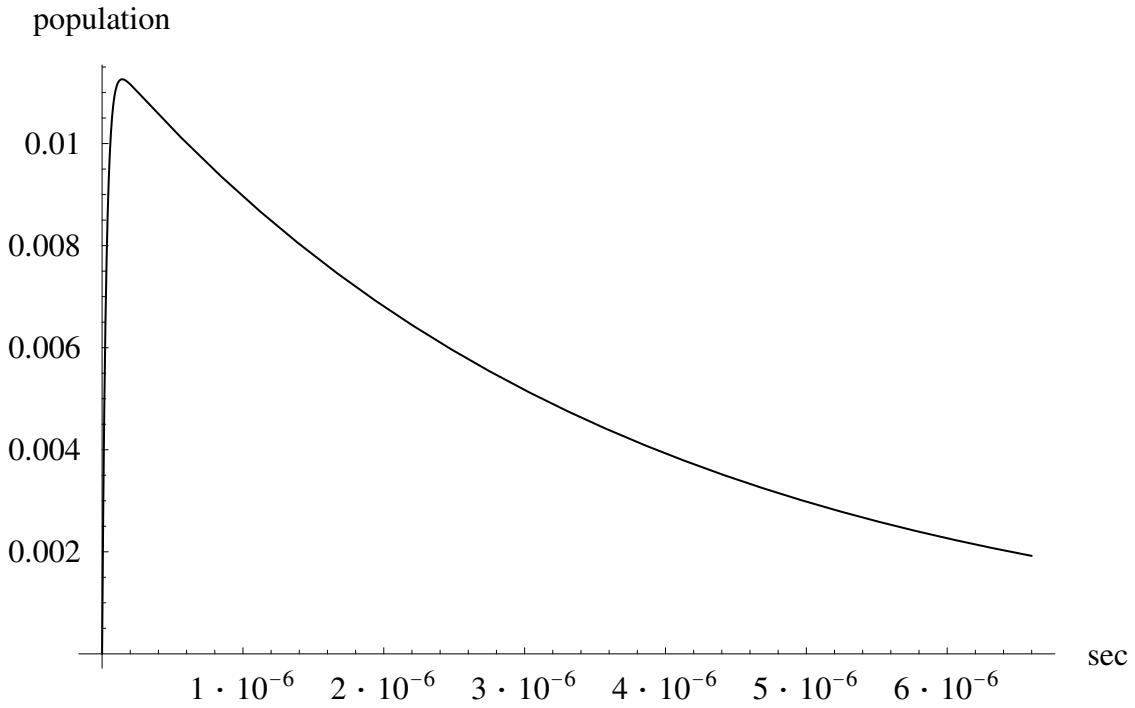

Figure 3.4: The population of $7S_{1/2}$ $(F = 0)$ state varies with times.

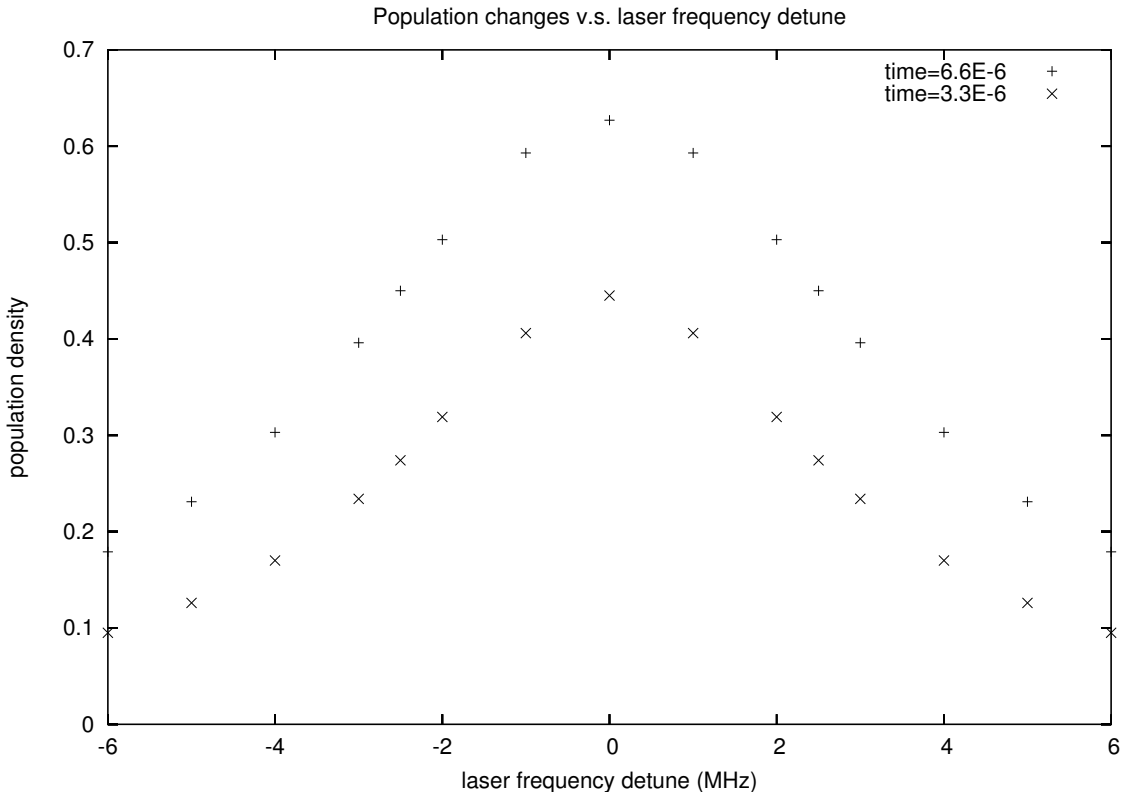

Figure 3.5: The signal strength v.s. laser detune

Table 3.2: Hyperfine splittings and isotope shift. All results are in MHz

	^{205}Tl $6P_{1/2}$	^{203}Tl $6P_{1/2}$	^{205}Tl $7S_{1/2}$	^{203}Tl $7S_{1/2}$	IS of $6P_{1/2} \rightarrow 7S_{1/2}$
This work	21311.4(9)	21105.6(7)	12295.4(6)	12180.2(7)	1658.8(6)
Ref.[25]			12294.5(1.5)	12180.5(1.8)	1659.0(6)
Ref.[26]			12297.2(1.6)	12181.6(2.2)	
Ref.[27]			12284.0(6.0)	12172.0(6.0)	
Ref.[28]			12318(36)	12225(42)	
Ref.[29]	21310.835(5)	21105.447(5)			
Theor.[9]	21663		12666		
Theor.[13]	21300		12760		
Theor.[30]	21623		12307		

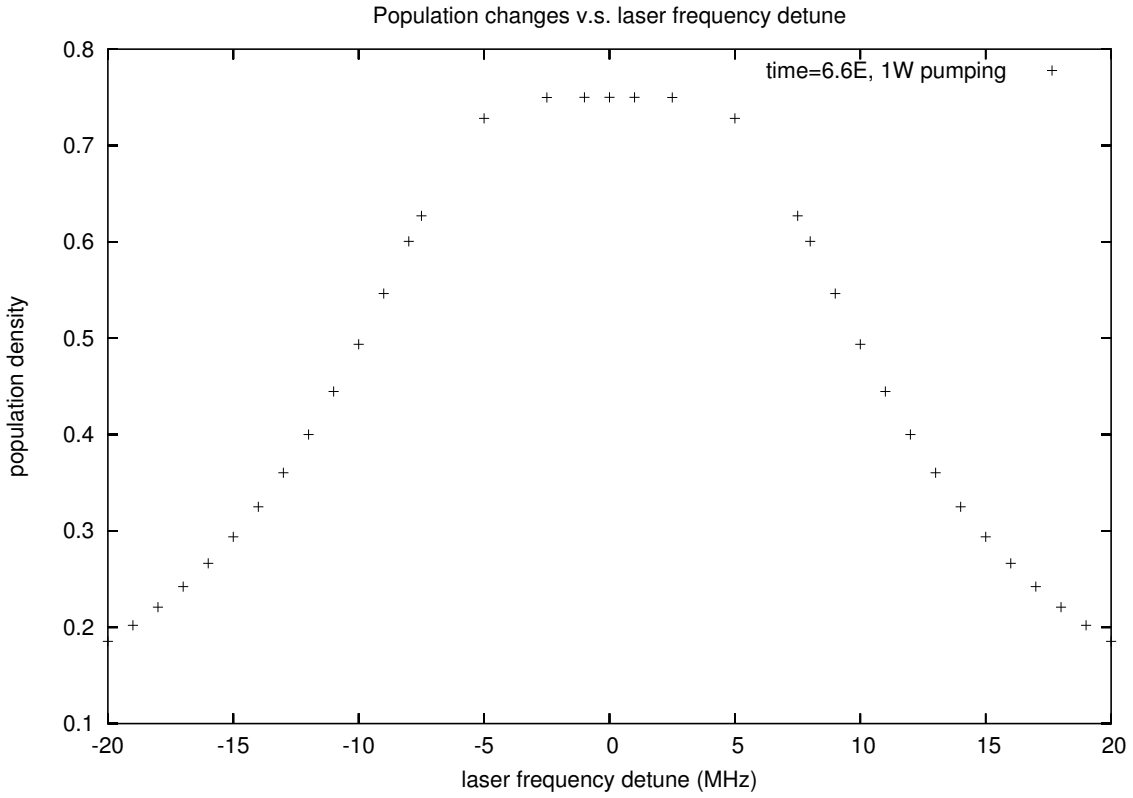

Figure 3.6: The signal strength v.s. laser detune

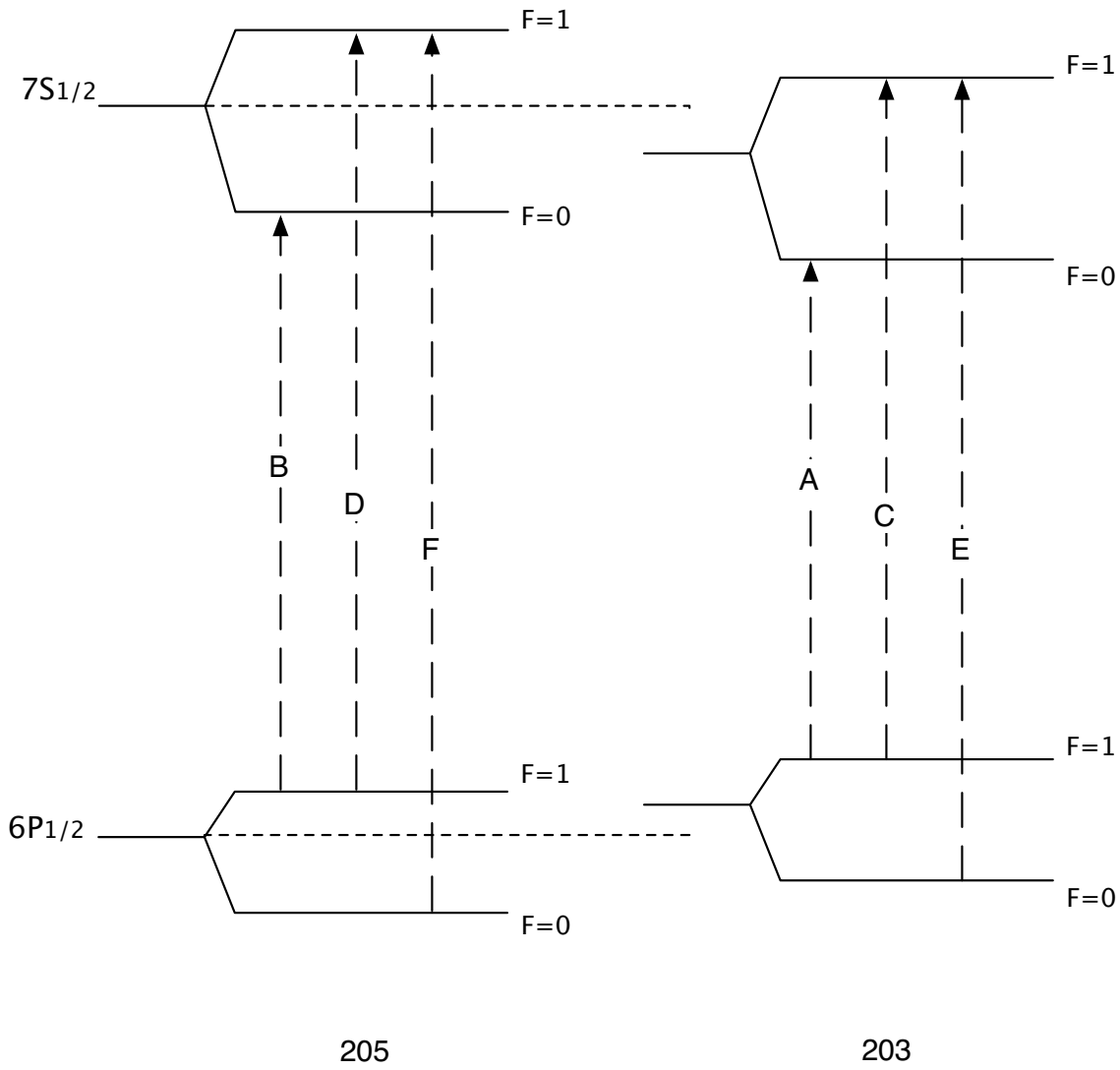

Figure 3.7: Energy levels within the $6P_{1/2} \rightarrow 7S_{1/2}$ transition in ^{203}Tl and ^{205}Tl. The six lines are labeled A–F for identification on Table. 3.1

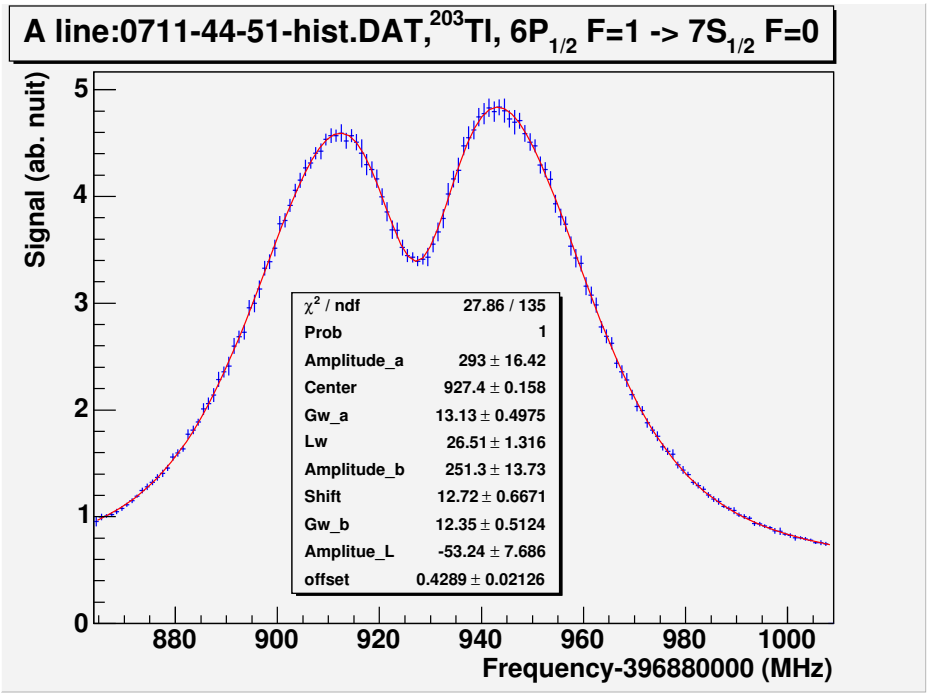

Figure 3.8: Fitting result of A line

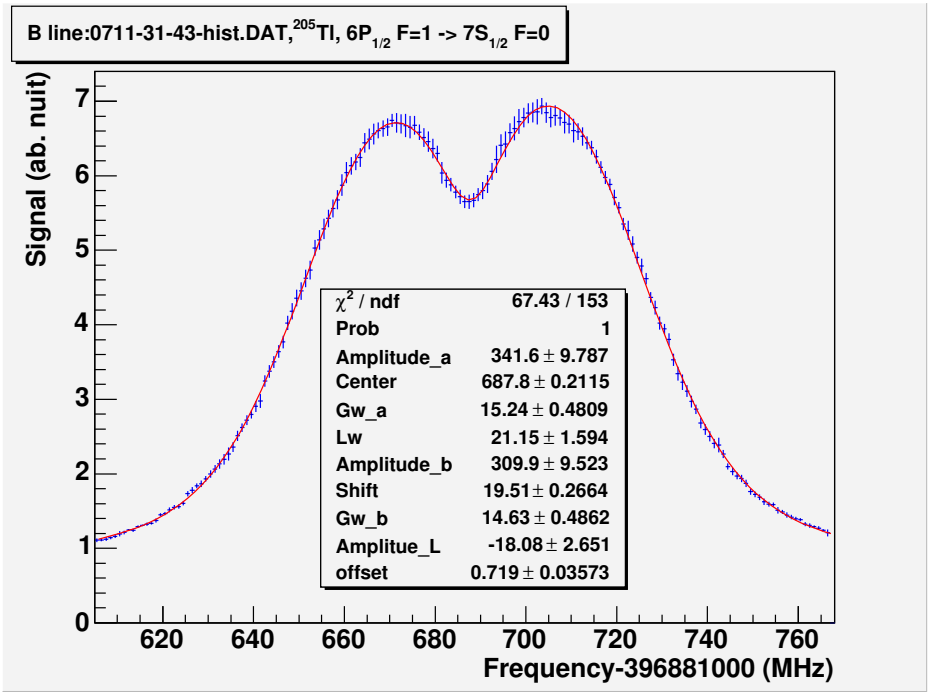

Figure 3.9: Fitting result of B line

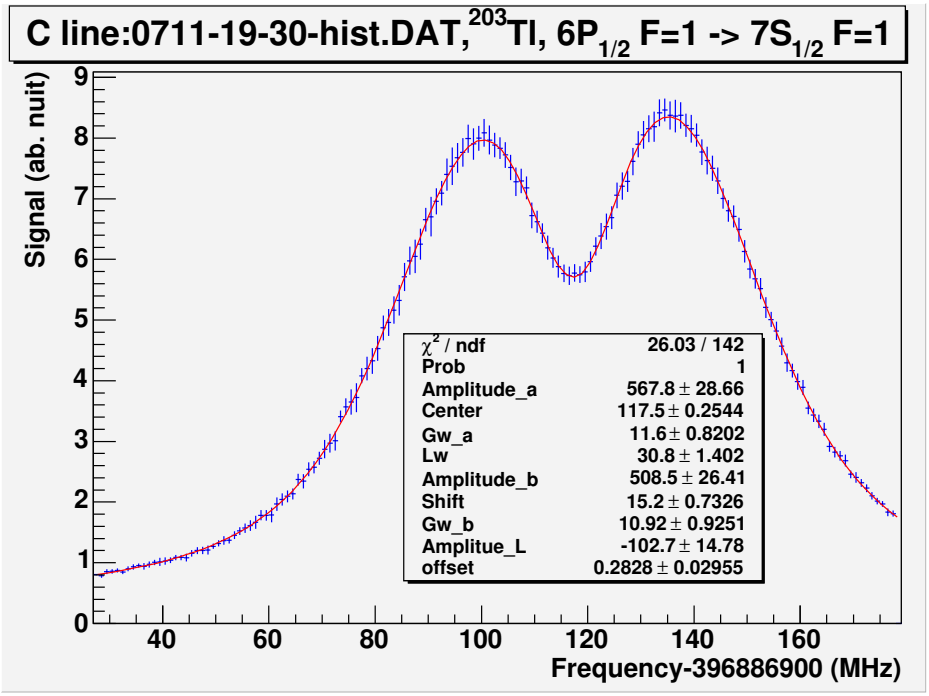

Figure 3.10: Fitting result of C line

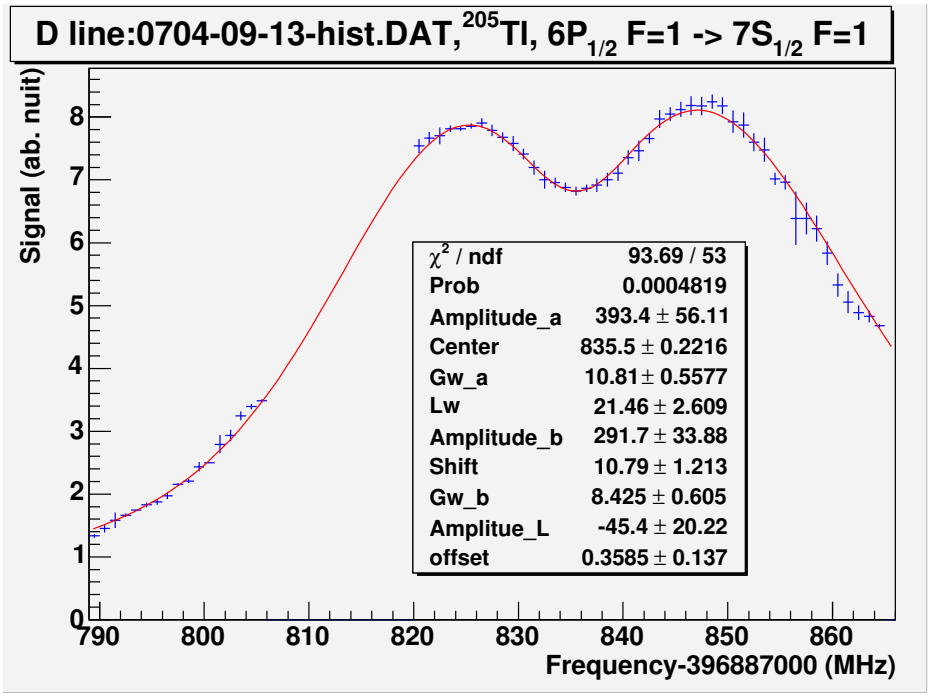

Figure 3.11: Fitting result of D line

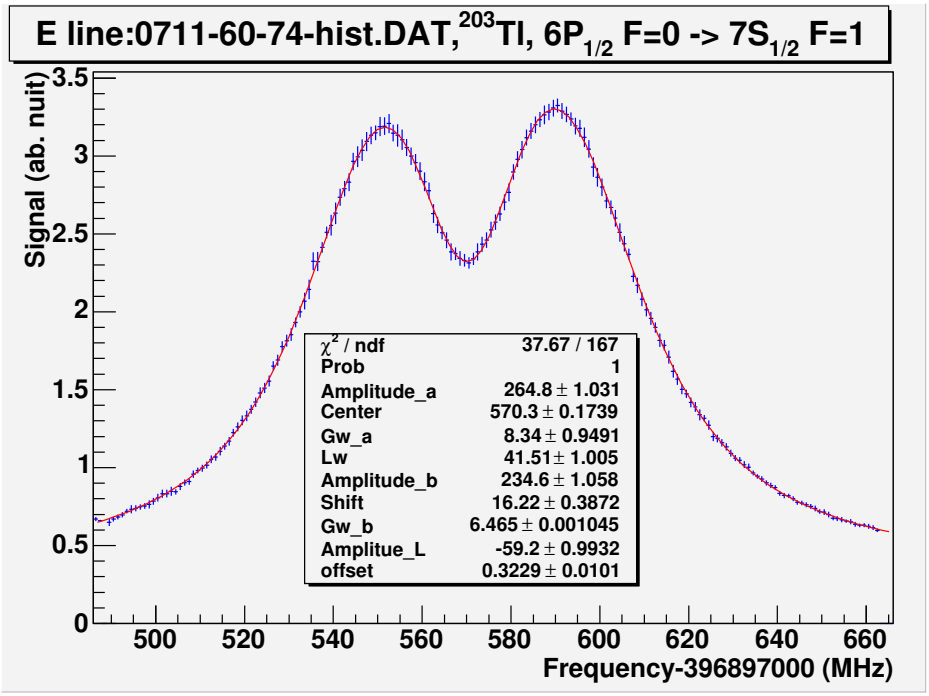

Figure 3.12: Fitting result of E line

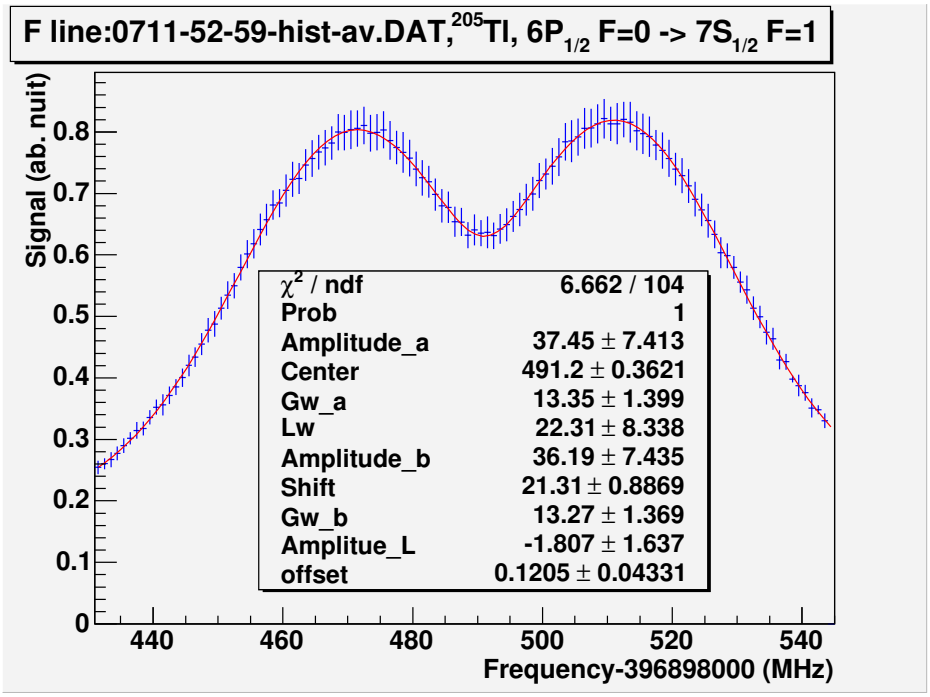

Figure 3.13: Fitting result of F line

$1.63821461\mu_N$, we find that

$$\Delta = -3.7(0.8) \times 10^{-4} \ .$$

As shown in [13], this experimental quantity can be combined with nuclear structure calculations regarding the magnetic moments and charge distributions in the isotope to infer a value for the mean square isotopic *change* in these distributions, referred to as $\lambda_{c,m}$ in [13]. We infer

$$\lambda_{c,m} = 0.49(10) \text{ fm}^2$$

based on our experimental results and this theoretical model. The equivalent derivation based on the results for the $7S_{1/2}$ state HFS reported in [25] gives $\lambda_{c,m} = 0.61(20)$ fm^2 and $\lambda_{c,m} = 0.45(24)$ fm^2 in [26]. The quoted uncertainty in $\lambda_{c,m}$ reflects experimental errors only.

Our result for ^{205}Tl $-^{203}$ Tl transition isotope shift [$\delta\nu_{205-203} = 1658.8(6)$ MHz] is not prior to [25] [$\delta\nu_{205-203} = 1659.0(6)$ MHz] because our experimental error contains the ground state measurement. Using the value for the ground-state level isotope shift (LIS) relative to the ionization limit derived in [26] of $-1250.0(3.8)$ MHz, our result allows us to infer a value of $+408.8(3.8)$ MHz for the thallium $7S_{1/2}$-state LIS. Combining our result for the 377-nm transition with the precise measurement of the thallium $6P_{3/2} - 7S_{1/2}$ 535-nm transition isotope shift (TIS) [$\delta\nu_{205-203} = 1757.3(4)$ MHz] [26], we can deduce the value of $\delta\nu_{205-203} = -98.5(7)$ MHz for the TIS of thallium $6P_{1/2} - 6P_{3/2}$ 1283-nm $M1$ transition.

Chapter 4

Conclusions

Conclusions

Absolute frequencies of thallium $6P_{1/2} \rightarrow 7S_{1/2}$ transition (377-nm) have been measured to an accuracy of 0.4 MHz (1 ppb) using the optical femtosecond comb by centering the lamb dip using two counter-propagating laser beams perpendicular to the atomic beam. The hyperfine splitting of thallium $7S_{1/2}$ state is improved by a factor of 2 in this measurement, comparing with previous best results.

Future work

In the future, possible works are listed below:

1. The doubling efficiency should be increased.

2. Decrease the linear Doppler shift by adjusting the angle between laser and atomic beams, and the saturation effect (Lamb dip) could be more pronounced. Using an external cavity diode laser as fundamental laser source and stabilizing the frequency onto the Lamb dip, the accuracy of absolute frequency measurement could be achieved 20 kHz.

3. The $6P_{3/2} \rightarrow 6D_{5/2}$ 351-nm transition has been also observed with another frequency-doubled light of a 702-nm Ti-sapphire. Using the optical femtosecond comb measure the absolute frequencies of thallium $6P_{3/2} \rightarrow 6D_{5/2}$ transition

(351-nm) and $6P_{3/2} \rightarrow 6D_{3/2}$ transition (350-nm).

4. The 377-nm laser can optically pump the atom to $6P_{3/2}$ states and excite $6P_{3/2}$ to $6D_{5/2}$ transition using 351-nm light source. The further purpose is to realize laser cooling technique taking advantage of the close transition cycle of $F = 2 \rightarrow F = 3$.

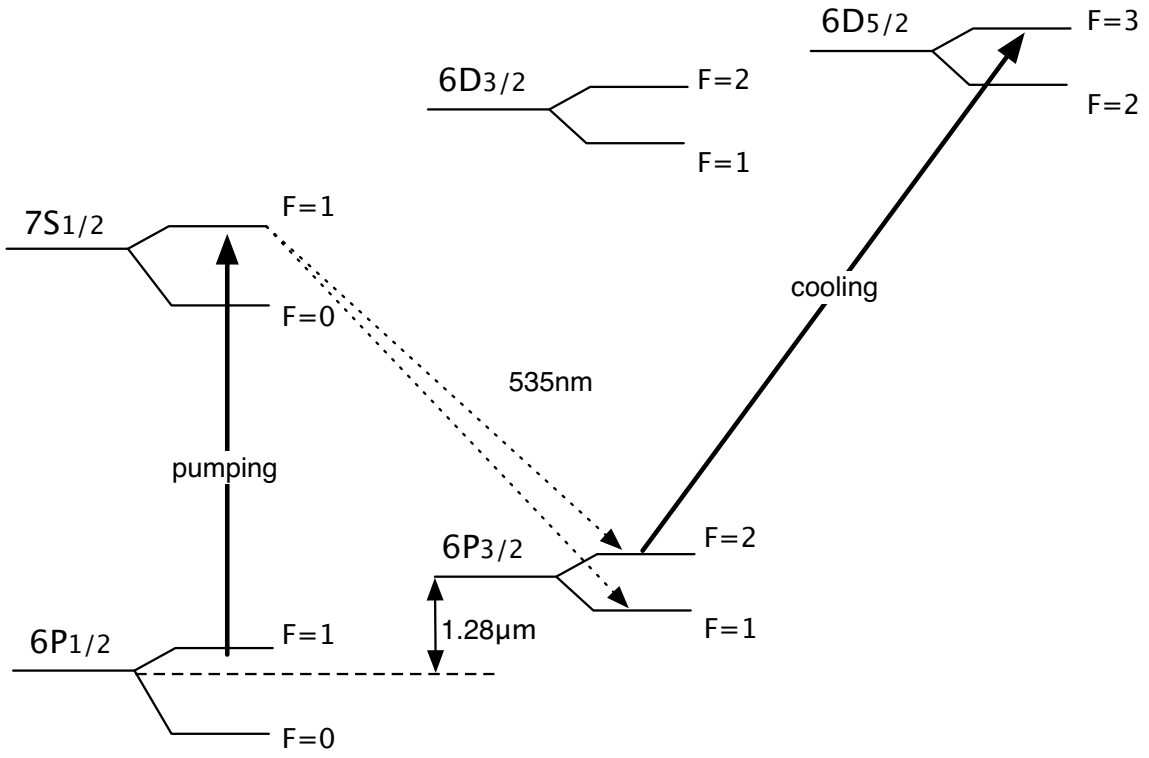

Figure 4.1: Level diagram showing the low-lying atomic structure in Tl. The cooling transition used is from the metastable state $6P_{3/2}(F = 2)$ to $6D_{5/2}(F = 3)$.

Appendix A

ROOT Program for Data Fitting

```
#include "Riostream.h"

Double_t rvoigt(Double_t *x, Double_t *par){

        Double_t temp_a=par[0]*TMath::Voigt(x[0]-par[1]-par[5],par[2],par[3],5);
        Double_t temp_b=par[4]*TMath::Voigt(x[0]-par[1]+par[5],par[6],par[3],5);
        Double_t temp_lo=(2*par[7]*par[3])/(TMath::Power(par[3],2) +
             4*TMath::Power(par[1] - x[0],2));

            Double_t temp_all=temp_a+temp_b+temp_lo+par[8];

            return temp_all;
};

void A_fixLW()       //Filename must be "A_fixLW.c"
{
   gROOT->Reset();

   gStyle->SetOptStat(0000000);
   gStyle->SetOptFit(1111);
   gStyle->SetTitleW(0.6);
   gStyle->SetTitleH(0.08);

   ifstream in;
   in.open("/Users/imac/Desktop/Tl-frequency-final/0711-44-51-hist.DAT");

   Double_t x,y,z;

   Int_t num=0;
   Int_t nlines=0;

   Double_t xo_start=396880864;
```

```
   Double_t x_length=145;
   Double_t gap;
   Int_t bins=145;
   Double_t offset_f=396880000;
   Double_t x_start=xo_start-offset_f;

   gap=x_length/bins;

   TH1F *h1 = new TH1F("h1","A line, ^{203}Tl,6P_{1/2} F=1 -> 7S_{1/2}F=0",
            bins,x_start,x_start+x_length);

   while (1) {
      in >> x >> y >> z;
      if (!in.good()) break;
      num=floor((x-offset_f-x_start)/gap+0.5);
      if (nlines < 10) printf("x=%12f, y=%12f, z=%12f, num=%d\n",x,y,z, num);

      h1->SetBinContent(num,y);
      h1->SetBinError(num,z);
      nlines++;
   }
   printf(" found %d points\n",nlines);

   in.close();

   TCanvas *c1 = new TCanvas("c1","the fit canvas",800,600);

   TF1 *myvoigt = new TF1("myvoigt",rvoigt,x_start,x_start+x_length,9);

myvoigt->SetParName(0,"Amplitude_a"); myvoigt->SetParameter(0,200);
//   myvoigt->FixParameter(0,660);

myvoigt->SetParName(1,"Center"); myvoigt->SetParameter(1,935);
//   myvoigt->FixParameter(1,935);

myvoigt->SetParName(2,"Gw_a"); myvoigt->SetParameter(2,15);
//   myvoigt->FixParameter(2,10);

myvoigt->SetParName(3,"Lw"); myvoigt->SetParameter(3,5);
   myvoigt->FixParameter(3,5);

myvoigt->SetParName(4,"Amplitude_b"); myvoigt->SetParameter(4,200);
//   myvoigt->FixParameter(4,388);

myvoigt->SetParName(5,"Shift"); myvoigt->SetParameter(5,10);
```

```
//  myvoigt->FixParameter(5,0);

myvoigt->SetParName(6,"Gw_b"); myvoigt->SetParameter(6,15);
//   myvoigt->FixParameter(6,11);

myvoigt->SetParName(7,"Amplitue_L"); myvoigt->SetParameter(7,-20);
//   myvoigt->FixParameter(8,-230);

myvoigt->SetParName(8,"offset"); myvoigt->SetParameter(8,0.5);
//   myvoigt->FixParameter(10,0);

myvoigt->SetLineColor(2);
myvoigt->SetLineWidth(1);
myvoigt->SetLineStyle(1);

h1->Fit("myvoigt","R");

   h1->SetLineWidth(1);
   h1->SetLineColor(4);
   h1->SetXTitle("Frequency-396880000 (MHz)");
   h1->SetYTitle("Signal (ab. unit)");

};
```

Appendix B

Setup of Optical Frequency Comb

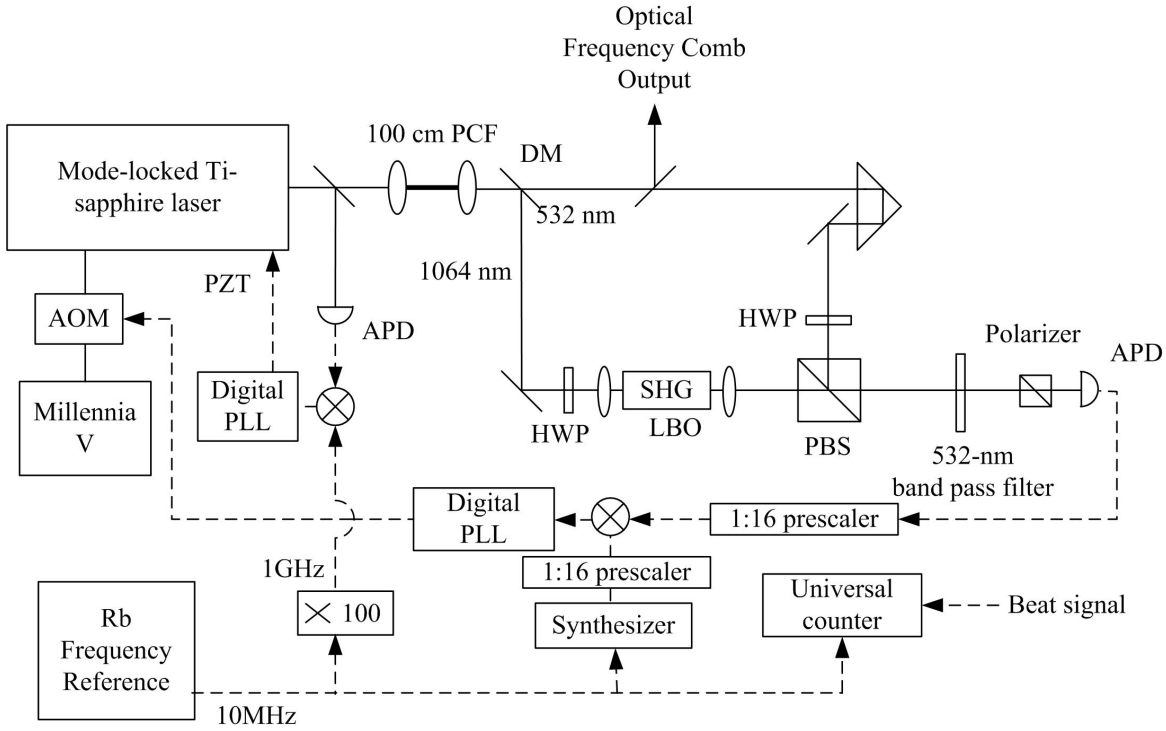

References

[1] M. J. D. Macpherson *et al.*, Phys. Rev. Lett. **67**, 2784 (1991).

[2] D. M. Meekhof *et al.*, Phys. Rev. Lett. **71**, 3442 (1993).

[3] S. J. Phipp, N. Edwards, P. Baird, and S. Nakayama, J. Phys. B **29**, 1861 (1996).

[4] P. A. Vetter *et al.*, Phys. Rev. Lett. **74**, 2658 (1995).

[5] N. H. Edwards, S. J. Phipp, P. E. G. Baird, and S. Nakayama, Phys. Rev. Lett. **74**, 2654 (1995).

[6] C. S. Wood *et al.*, Science **275**, 1759 (1997).

[7] S. A. Blundell, J. Sapirstein, and W. R. Johnson, Phys. Rev. D **45**, 1602 (1992).

[8] V. A. Dzuba, V. V. Flambaum, and O. P. Sushkov, Phys. Lett. A **141**, 147 (1989).

[9] M. G. Kozlov, S. G. Porsev, and W. R. Johnson, Phys. Rev. A **64**, 052107 (2001).

[10] F. N, S. P, and B. S, Physics Today **56(6)**, 33 (2003).

[11] J. Ginges and V. Flambaum, Phys. Rep. **397**, 63 (2004).

[12] A.-M. Martensson-Pendrill and A. C. Hartley, J. Phys. B **24**, 1193 (1991).

[13] A.-M. Mårtensson-Pendrill, Phys. Rev. Lett. **74**, 2184 (1995).

[14] S. PGH, Contemp. Phys. **42**, 97 (2001).

[15] A. Radzig and B. Smirnov, *Reference Data on Atoms, Molecules, and Ions* (Springer-Verlag, New York, 1985).

[16] W. Demtroder, *Laser spectroscopy : basic concepts and instrumentation*, 3rd ed. (Springer, New York, 2003).

[17] T. Udem, R. Holzwarth, and T. W. Hänsch, Nature **416**, 233 (2002).

[18] LBO crystal purchased from Fujian Castech Crystals, Inc.

[19] B. Couillaud and T. W. Hänch, Opt. Comm. **35**, 441 (1980).

[20] *Atomic and Molecular Beam Methods*, 1st ed., edited by G. Scoles, D. Bassi, U. Buck, and D. Lainé (Oxford University Press, New York, 1998).

[21] S.-M. Yang, Master's thesis, National Tsing Hua University, 2004.

[22] H.-C. Chui, Ph.D. thesis, National Tsing Hua University, 2004.

[23] C.-H. Ho, Master's thesis, National Tsing Hua University, 2004.

[24] Kurucz, Atomic spectral line database from Kurucz files, http://cfa-www.harvard.edu/amdata/ampdata/kurucz23/sekur.html.

[25] D. S. Richarson, R. N. Lyman, and P. K. Majumder, Phys. Rev. A **62**, 012510 (2000).

[26] G. Hermann, G. Lasnitschka, and D. Spengler, Z. Phys. D **28**, 127 (1993).

[27] R. Neugart, Phys. Rev. Lett. **55**, 1559 (1985).

[28] C. Schuler, M. Ciftan, L. B. III, and H. Stroke, J. Opt. Soc. Am. **52**, 501 (1962).

[29] A. Lurio and A. G. Prodell, Phys. Rev. **101**, 79 (1956).

[30] V. A. Dzuba, V. V. Flambaum, M. G. Kozlov, and S. G. Porsev, J. Exp. Theor. Phys. **87**, 885 (1998).

[31] P. Raghavan, At. Data and Nucl. Data Tables **42**, 189 (1989).